

Lawrence Berkeley National Laboratory

LBL Publications

Title

Landslide activation behaviour illuminated by electrical resistance monitoring

Permalink

<https://escholarship.org/uc/item/4qs4c26f>

Journal

Earth Surface Processes and Landforms, 43(6)

ISSN

0197-9337

Authors

Merritt, AJ
Chambers, JE
Murphy, W
[et al.](#)

Publication Date

2018-05-01

DOI

10.1002/esp.4316

Peer reviewed

Landslide activation behaviour illuminated by electrical resistance monitoring

A.J. Merritt, J.E. Chambers, W. Murphy, P.B. Wilkinson, L.J. West, S. Uhlemann, P.I. Meldrum, D. Gunn

Abstract

A common factor in landslide activation (or reactivation) is subsurface moisture and associated pore pressure variations linked to rainfall. Monitoring of these subsurface hydrogeological processes is necessary to improve our understanding of water-induced landslide activation. Geophysical approaches, electrical methods in particular, are increasingly being applied to landslide monitoring because they provide non-invasive spatial information in heterogeneous subsurface environments that can be difficult to characterise using surface observations or intrusive sampling alone. Electrical techniques are sensitive to changing subsurface moisture conditions, and have proven to be a useful tool for investigating the hydrogeology of natural and engineered slopes.

The objectives of this investigation were to further develop electrical resistance monitoring for slope stability assessment, and to validate the approach at an intermittently-active UK landslide system to advance the understanding of complex landslide activation mechanisms. A long-term transfer resistance dataset was collected from a grid of electrodes to allow spatial monitoring of the landslide. These data were interpreted using a synthesis of rainfall, temperature, GPS and piezometric records. The resistance data were corrected for seasonal temperature variations and electrode movements were monitored, as these processes were shown to mask moisture related changes. Results reveal that resistance monitoring is sensitive to soil moisture accumulation, including changes in piezometric levels, and can be used to study the principal activation mechanism of slow-moving shallow earthflows. Spatial monitoring using resistance maps was shown to be particularly valuable as it revealed the evolution of subsurface moisture distribution, in the lead up to landslide activation.

Key benefits of this approach are that it provides a simple, rapid and non-invasive means of spatially monitoring subsurface moisture dynamics linked to landslide activation at high-temporal resolution. Crucially, it provides a means of monitoring subsurface hydraulic changes in the build-up to slope failure, thereby contributing to early warning of landslide events.

Introduction

If the effects of landslides are to be mitigated and avoided then landslide activation and re-activation mechanisms must be better understood. One way of developing a better understanding of landslide activation events is by monitoring subsurface changes during the period leading to activation. The most common change in the subsurface leading to activation (or

reactivation) is the movement of water and associated pore pressure variations, which in turn are closely linked to antecedent rainfall conditions (Moore *et al.*, 2007; O'Brien *et al.*, 2007).

If changes in slope hydrogeology can be observed in advance of activation then an early warning of slope movement may be possible. The moisture content, and therefore propensity to fail, of natural soils is directly affected by climatic, seasonal and environmental factors such as rainfall amount and intensity, as well as evapotranspiration. Intense rainfall and rapid infiltration is widely accepted as one of the principal landslide triggers as slope materials show a reduction in mobilised strength with changing water pressure and associated effective stresses (Friedel *et al.*, 2006; Dijkstra and Dixon, 2010; Dijkstra *et al.*, 2014). In addition, a major contributing factor in clay slope instability is the dissipation of pore suction associated with elevated moisture content (Lourenco *et al.*, 2011; Toll *et al.*, 2011; Merritt *et al.*, 2016).

Many landslide warning systems rely on the use of rainfall thresholds (Tiranti and Rabuffetti, 2010; Reid *et al.*, 2012; Papa *et al.*, 2013; Segoni *et al.*, 2015), but there is a growing appreciation that direct observation of water in the subsurface is also desirable (Intrieri *et al.*, 2013; Stahli *et al.*, 2015). This is because the link between rainfall events and failure can be complex, requiring an understanding of both long-term antecedent weather conditions and subsurface heterogeneity (Dijkstra and Dixon, 2010; Take and Bolton, 2011). In recent years monitoring of landslide processes by geoelectrical methods has become more common (Perrone *et al.*, 2014). Examples include short-term studies using electrical resistivity tomography (ERT) to intensively monitor simulated rainfall events on vulnerable slopes to determine subsurface moisture variation in controlled conditions (Travelletti *et al.*, 2012; Lehmann *et al.*, 2013). Studies using ERT to monitor landsliding under natural conditions over a period of months have revealed the link between subsurface moisture distribution and rainfall, and demonstrated the ability of this approach to observe dynamic and complex hydrogeological processes in landslide systems (Lebourg *et al.*, 2005, 2010; Jomard *et al.*, 2007; Bièvre *et al.*, 2012; Supper *et al.*, 2014; Gance *et al.*, 2016). Longer term multi-year studies have also been described. Uhlemann *et al.* (2017) describe the use of four-dimensional ERT to monitor an active landslide over a 3 year period, showing the relationship between increasing subsurface moisture content and failure events. However, the high spatial and temporal resolution presented here focuses on shallow landslide (re)activation to place emphasis on the movement patterns of the type of landslide commonly affecting infrastructure assets (Loveridge *et al.*, 2010). Palis *et al.* (2017) used three-dimensional (two-dimensional (2D) image plus time) ERT monitoring over a 2 year period to distinguish between moisture driven processes above and below the base of the landslide. In addition, and of particular relevance to this study, they correlated raw apparent resistivity measurements (i.e. unprocessed measurements) from their 2D line of ERT electrodes with

subsurface moisture changes associated with individual rainfall events as well as longer term seasonal changes. These previous investigations reveal that time-lapse electrical measurements are a useful tool to observe hydrogeological processes due to their sensitivity to moisture content variation, and therefore have the potential to provide information on moisture driven landslide activation mechanisms.

The aim of this study is to investigate the benefits of applying a multi-sensory system, incorporating novel-geophysical monitoring, which records in near-real-time both environmental inputs and the resulting subsurface response. Presented here are the results of nearly 5 years of high-temporal resolution geoelectrical and environmental monitoring of a periodically active inland landslide located within landslide-prone Liassic rocks of the UK – representing one of the longest-term geophysical monitoring studies of an active landslide. To the best of our knowledge this is the only study where spatially distributed (i.e. using a grid of electrodes rather than a linear array) raw electrical resistance data have been used to monitor an active landslide using fully automated data acquisition. The overarching objective of this investigation is to utilise electrical resistance monitoring measurements to advance the understanding of complex landslide activation mechanisms, and is achieved through integration and analysis of monitoring campaign results. The sensitivities and benefits of using rapidly-generated resistance measurements, that only require minimal manipulation and without time-consuming inversion modelling are highlighted.

Hollin Hill study site

The study site is a landslide located in the UK county of North Yorkshire 20 km north of York and 11 km west of Malton (Dixon *et al.*, 2014; Merritt *et al.*, 2014), Ordnance Survey grid reference SE672706. It is situated on a south-facing slope approximately 450 m by 200 m, which is used as pasture. The slope is approximately 50 m high from the base to the top of the slope (mean slope angle of 12°). Beyond the base of the hillslope is a wide topographic embayment. The slope is composed of four geological formations of Lower and Middle Jurassic Age (Figure 1). The base of the Hollin Hill slope is formed of Redcar Mudstone Formation (RMF) and marks the oldest formation at the field site. This is overlain by Staithes Sandstone Formation (SSF) which gives way to Whitby Mudstone Formation (WMF), with Dogger Formation (DGF) capping the hill slope.

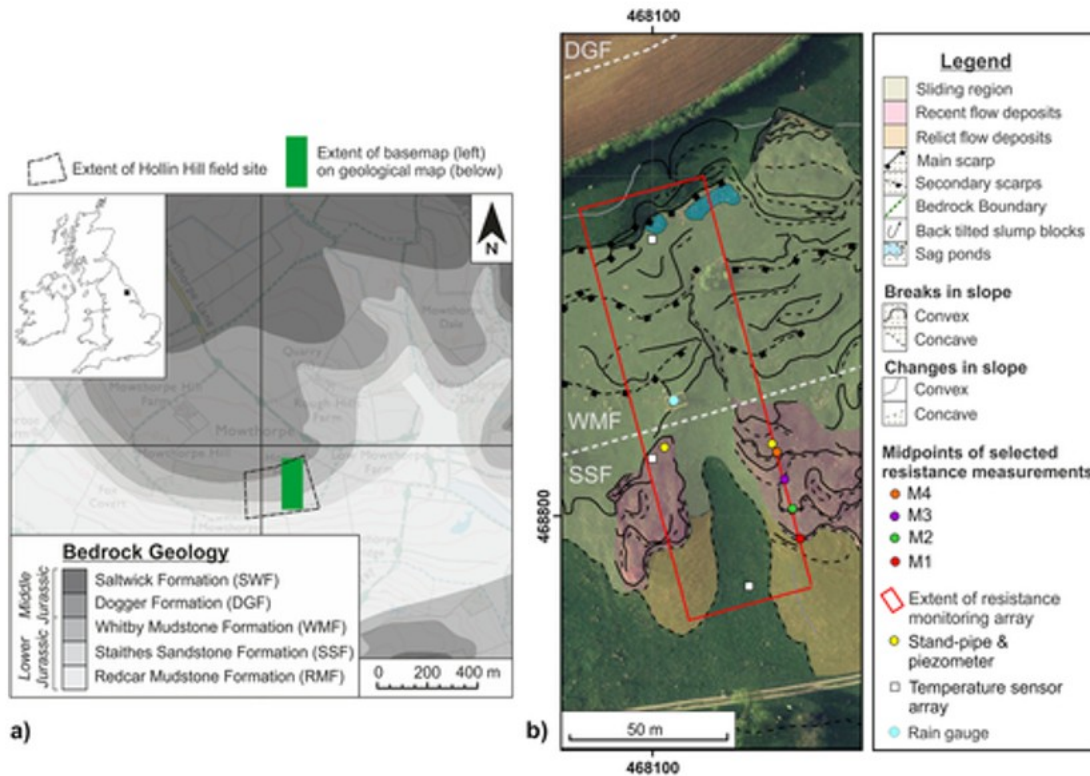


Figure 1

(a) Geological map of the study area and inset large-scale map. (b) Engineering geomorphological map of study site. The depths of the sensors within the temperature sensors arrays are as follows: northern array - 0.1, 1.0, 2.5, 5.35 m; middle array - 0.1, 0.7, 2.0, 3.8, 6.4 m; southern array - 0.1, 0.7, 2.0, 3.8, 6.4 m. Coordinate system used is British National Grid. Figure is amended from Merritt *et al.* (2014). BGS © NERC. Contains Ordnance Survey data © Crown Copyright and database rights 2016.

Present at the study site is a complex landslide system that exhibits a variety of landslide types and activity, with WMF being the most susceptible to instability (Jones and Lee, 1994; Foster *et al.*, 2007). The landslide system extends ~250 m laterally along the hill slope beyond the limits of the study site. Several types of slope failure can be observed at the test site, with the landslide system described as ‘a very slow to slow moving multiple earth slide - earth flow’ (Chambers *et al.*, 2011). The whole system would correctly be referred to as a complex landslide (Cruden and Varnes, 1996). However, as the focus of this study requires the differentiation between earthflow and earthslide regions of the landslide system, the landslide will be referred to using this terminology.

The landslide system has been the focus of previous geotechnical and geophysical investigations (Chambers *et al.*, 2011; Gunn *et al.*, 2013), including assessment of landslide structure, activation timings (Smith *et al.*, 2014; Uhlemann *et al.*, 2015b), conceptual model development (Merritt *et al.*, 2014) and ERT monitoring (Uhlemann *et al.*, 2017). The earthflow region of this landslide system is the most frequently active (Figures 1 and 2), with movement rates of up to 3.5 m per year observed since monitoring began in

2008 (Uhlemann *et al.*, 2017). The earth flows are composed of highly weathered WMF, characterised as a high plasticity clay, with a thickness of up to approximately 5 m (Merritt *et al.*, 2014). Failure surfaces are predominantly within the upper 2 m of the earth flows, but there is evidence of deeper failure surfaces at the base of the earthflows (Uhlemann *et al.*, 2015b).

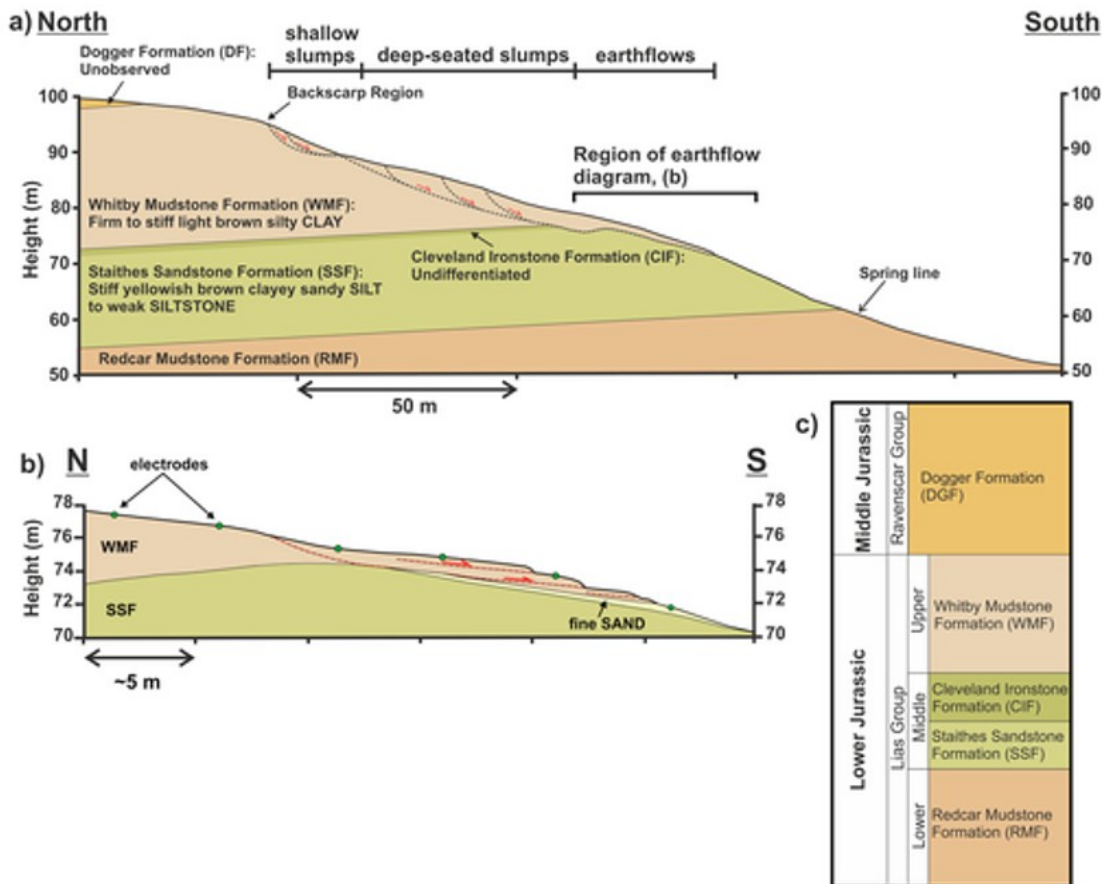


Figure 2

Cross-sections of the complex landslide system at the Hollin Hill Test Site; (a) ground model of overall geometry of landslide system (adapted from Uhlemann *et al.* (2015b)); (b) Detailed ground model of earthflow regions (western flow region represented). Ground model represented as Figure 2(a) extends from beyond the landslide crown, through the axis of an earthflow to the base of the hillslope.

Methodology

Time-lapse transfer resistance measurements

A permanently-installed geoelectrical monitoring system called Automated time-Lapse ERT (ALERT) developed by the British Geological Survey (Wilkinson *et al.*, 2010; Chambers *et al.*, 2015) was deployed on site. The remotely configurable system can be interrogated by wireless telemetry from the office via GSM (GPRS or 3G) or wireless internet link. Via this link pre-programmed data acquisition schedules are uploaded and measurement results downloaded. The system is powered by high-capacity batteries which

are recharged by a combination of wind-turbine, solar panels and a methanol fuel cell. The ALERT sensor arrays were arranged in five parallel lines each comprising 32 stainless steel electrodes, creating a grid of 160 electrodes. The electrodes were located 0.1 m below the ground surface. Electrode lines are orientated downslope, i.e. 165°S, having a 9.5 m line spacing and 4.75 m electrode spacing. Thus, the monitoring grid covered an area of 147.25 m by 38 m. The ALERT system is designed to measure electrical transfer resistances using four-point measurements, comprising a current dipole (i.e. pair of electrodes) used to inject current, and a potential dipole that is used to measure the resulting potential difference. The system automatically undertakes measurements using predefined combinations of electrodes within the monitoring grid. Resistance measurements were acquired, using a standard dipole-dipole array configuration, on an alternating daily basis with occasional gaps due to system, battery, electrode array, or telemetry failure. The first resistance measurements were taken on 11/07/2008.

Electrode position interpolation

Electrode arrays at the study site are buried just below the ground surface. This was to prevent damage to the arrays by the livestock that graze the site. Consequently, when ground movement occurs the exact positions of the electrodes are not known; therefore a method to derive the best-estimate of electrode positions is required (Wilkinson *et al.*, 2010, 2015; Uhlemann *et al.*, 2015a).

An estimate of the location of electrodes, and therefore dipole-dipole measurement array size, is important when interpreting resistance measurements, so that resistance changes associated with movement can be differentiated from those associated with changing moisture conditions. Significant electrode movements (i.e. tens of cm) cause significant measurement variation, i.e. moving electrode closer together will lead to a smaller resistance, while moving them apart will lead to a higher measured resistance (Wilkinson *et al.*, 2010). Also, accurate electrode location information is required in the modelling steps used to temperature correct resistance measurements (see following section).

Electrode positions are estimated using a known set of reference points (i.e. a coarse grid of GPS benchmarks), following an approach by Uhlemann *et al.* (2015a). From the reference points the electrode locations can be estimated using a piecewise planar interpolation scheme, where movements are assumed to be represented by the location changes of three non-collinear reference points. Uhlemann *et al.* (2015a) show that by using this methodology, electrode movements can be estimated to about 10% of the electrode spacing, thereby removing significant movement related artefacts from the resistivity data.

Temperature correcting transfer resistances

Where time-lapse electrical resistance data are being compared over several months, it is important to correct measurements for the seasonal variation in subsurface temperature distribution (Hayley *et al.*, 2010). This is necessary because the electrical resistance of rock and soil is not only sensitive to moisture content, but also temperature (Brunet *et al.*, 2010). Therefore, without removing the effects of temperature variations from the electrical measurements it is difficult to differentiate between moisture and temperature driven changes.

The method used here to correct the time-lapse transfer resistance data for temperature variations is a two-stage process. First, the temperature variation within the subsurface is approximated by a simplified homogeneous model subject to a yearly sinusoidal temperature variation at the ground surface (Brunet *et al.*, 2010; Chambers *et al.*, 2014). The solution to the heat equation (Cannon, 1984) for this model is given by

$$T_{\text{MOD}}(z, t) = T_{\text{MAT}} + \frac{A}{2} e^{-\left(\frac{z}{d}\right)} \sin\left(\omega t + \varphi - \frac{z}{d}\right) \quad (1)$$

where T_{MOD} is the subsurface temperature at day t and depth z , T_{MAT} is the mean annual air temperature, A is the peak-to-trough magnitude of the annual air temperature variation, d is the characteristic depth of the temperature variation, φ is a constant phase offset, and ω is the angular frequency ($2\pi/365 \text{ day}^{-1}$). The constant phase offset ensures that the surface temperature is in phase with the air temperature. Seasonal subsurface temperature changes were recorded over a 2 year period using vertical arrays of temperature sensors at three locations on the landslide site (see Figure 1), and were fitted to Equation 1 to define the temperature model (Chambers *et al.*, 2014). The fitted parameters are listed in Table 1 along with the RMS misfits between the modelled and measured temperatures. Four separate models were fitted, one each for data from the individual locations and one for data combined from all three locations (which was the model used to correct the resistance data). For simplicity, the parameters were assumed to be independent of position and time. The misfit values are quoted for the 2 years of available data.

Table 1. Fitted parameters for the temperature models using data from the individual (T1,T2,T3) and combined locations (All), Equation (1)

Sensor Location	$T_{MAT} (^{\circ}C)$	$A (^{\circ}C)$	d (m)	ϕ (rad)	RMS ($^{\circ}C$)
T1	9.81	14.62	2.073	-1.907	0.88
T2	9.99	15.62	1.968	-1.908	0.84
T3	10.25	16.49	2.697	-1.896	1.02
All	10.03	15.54	2.264	-1.907	1.01

The second step is to correct the transfer resistances for the seasonal temperature variations. This involves assuming a linearised model for the variation of resistivity with temperature which is given by

$$\rho(T) = \rho(T_{MAT}) \left(1 + \frac{c}{100} (T - T_{MAT}) \right) \quad (2)$$

where c is the percentage resistivity change per °C, which is typically $c \approx -2.0^\circ\text{C}^{-1}$ (Hayley *et al.*, 2007). To calculate the temperature-corrected transfer resistance R_{tc} , it is assumed that the seasonal variations due to temperature changes are small compared with the overall range of the resistances due to the resistivity structure of the ground. This is a similar approach to that taken by Hayley *et al.* (2010). A further simplifying assumption is made that, for a given measurement configuration, the ratio of R_{tc} to the uncorrected (measured) resistance R can be approximated by

$$\frac{R_{tc}}{R} \approx \frac{R_h}{R_v} \quad (3)$$

where R_h and R_v are modelled transfer resistances for the same configuration. R_h is the transfer resistance resulting from a homogeneous half-space of resistivity ρ_h , and R_v is that resulting from a 1-D layered model where the variation of resistivity with depth is given by Equation (2) with $\rho(T_{MAT}) = \rho_h$ and $T = T_{MOD}$ as given by Equation 1. Ratio corrections such as these have previously been used to model the effects of other types of small perturbations (e.g. those due to topography, Tsourlos *et al.* (1999)). The use of a 1-D model allows the correction factors to be calculated rapidly (Ingeman-Nielsen and Baumgartner, 2006) as a function of time. Therefore, for each measurement configuration, the temperature-corrected transfer resistance is given by

$$R_{tc} = \frac{R_h}{R_v} R \quad (4)$$

The process of temperature correcting transfer resistance data for the analysis of subsurface physical processes adjusts raw data by $\pm 0.04 \Omega$, depending on whether modelled subsurface temperature is higher or lower than the averaged modelled subsurface temperature for the depth of interest. When comparing raw transfer resistance data with temperature corrected resistance data (e.g. Figure 3), it is apparent that the raw data varies much more seasonally, and is systematically higher in winter and lower in summer than temperature corrected data. There is a lag of ~ 1.5 months between weekly air temperature and resistance change ($\Delta\Omega$), which is due to the time taken for air temperature changes to propagate to the median depth of investigation (see Equation 1).

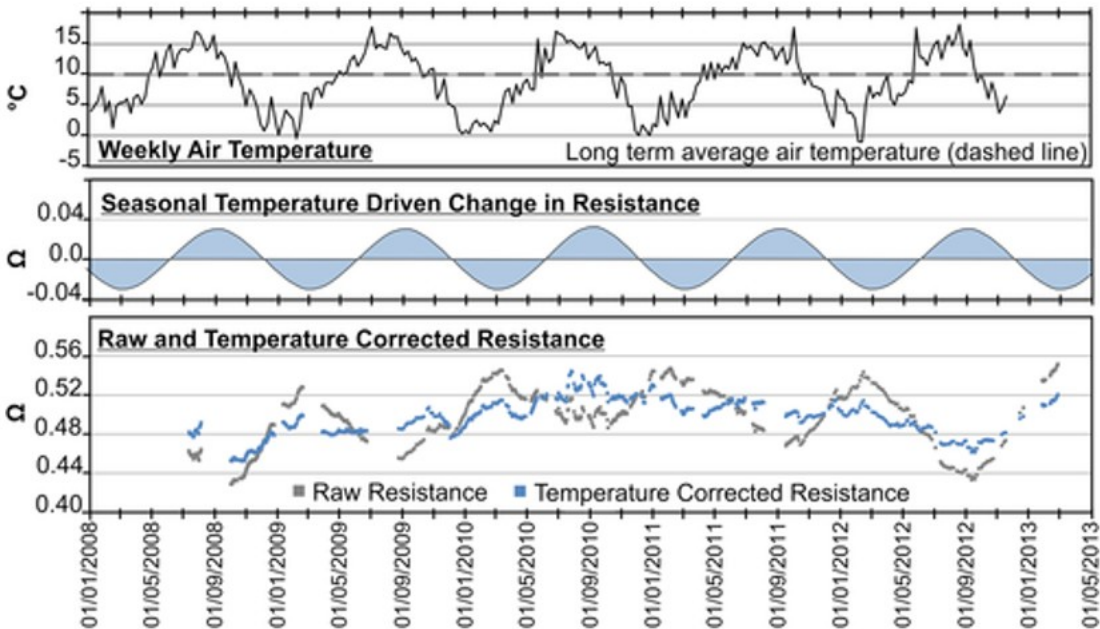


Figure 3

Quantifying temperature correction of transfer resistance datasets and seasonal air temperature variation. The example measurement shown here is located 19 m (x-axis), 95 m (y-axis), within sliding region.

Transfer resistance monitoring

The geoelectrical monitoring campaign comprised 695 geophysical surveys of all five lines during the four years and nine months of monitoring equating to 1740 days of monitoring, with ERT surveys performed on average every 2.5 days. The results of the geoelectrical monitoring campaign are a series of 'raw' transfer resistance measurements, which were corrected for the effects of subsurface temperature variation. Each dipole-dipole transfer resistance measurement presented here was performed using a four-electrode arrangement of adjacent electrodes, comprising two current (C) and two potential (P) electrodes arranged in the following order, C2-C1-P1-P2. Each four-electrode array had a length of 14.25 m and a median depth of investigation of 1.9 m. Measurements were performed using all available C2-C1-P1-P2 combinations of along each of the five lines.

Long-term temperature corrected resistance monitoring results are given as both 1D time-series from four selected dipole-dipole measurement locations (ML1, ML2, ML3, ML4 – Figures 4 and 6) and as 2D maps (Figure 7) using all resistance measurements made on the five lines of electrodes (with resistances plotted at the midpoints of each individual four-electrode measurement array). The results are presented as resistance ratios in Figures 4 and 6, and as resistance in Figures 7 and 8. Resistance ratio is the resistance at time t , normalised to the initial (or baseline) resistance measurement, and is a useful way of displaying how the measured resistances changed over time.

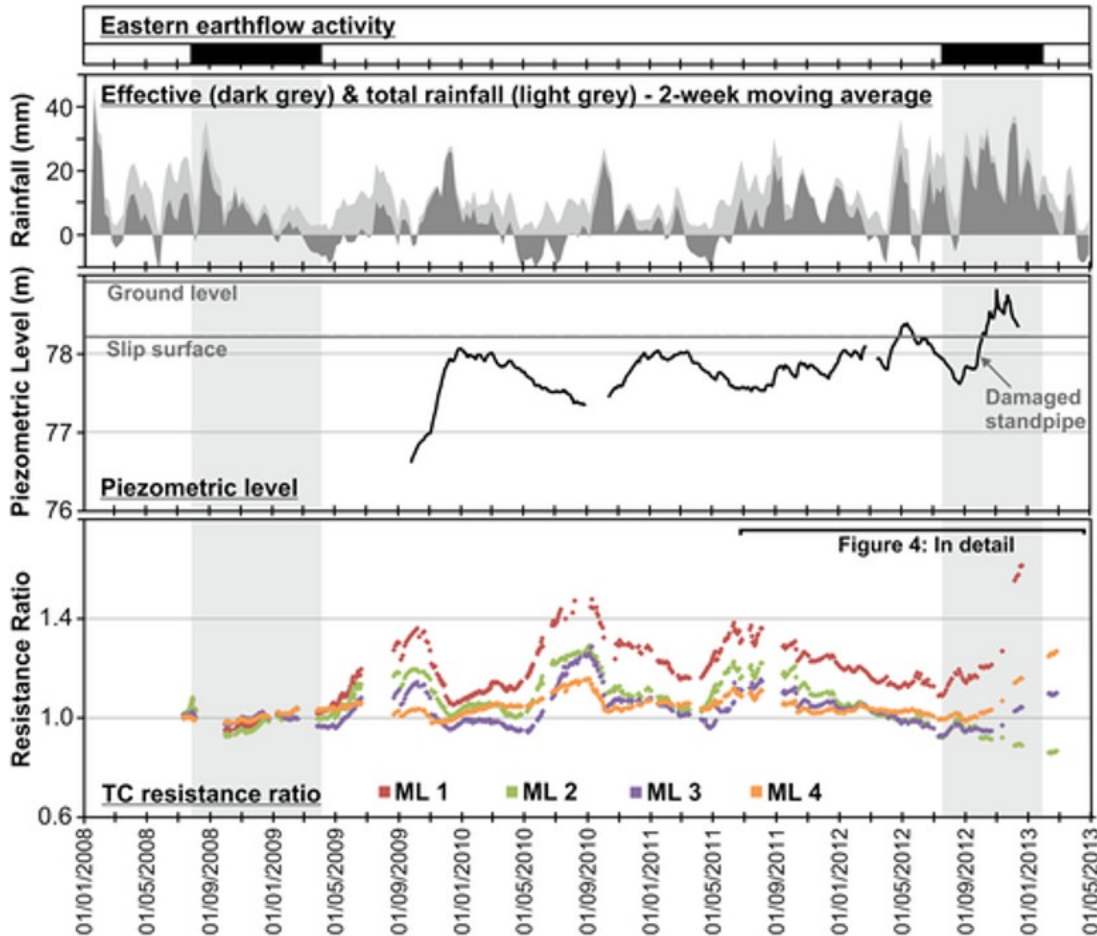


Figure 4

Goelectrical monitoring of landslide deposit results throughout the 4.75 year hill slope monitoring period (July 2008–March 2013). Subsurface ground conditions and environmental inputs are also presented in the form of piezometry and rainfall, respectively. NB: Piezometry and resistance data not present during several periods due to technical issues. Total rainfall refers to the observed rainfall at the site. Effective rainfall was calculated from the total rainfall using the Hargreave's method (Hargreaves and Allen, 2003), which accounts for the effects of evapotranspiration.

Environmental monitoring and modelling

Rainfall and evapotranspiration

Rainfall was monitored at the research site (see Figure 1(b) for rain gauge location) by 0.1 mm tipping-bucket type rain gauge to complement the results of the goelectrical monitoring regime with soil moisture input information. Rainfall data are presented as 2-week running mean (Figures 4 and 6), weekly total and weekly effective rainfall, with the latter requiring the estimation and removal of potential evapotranspiration effects, in mm/day, from total rainfall records using Hargreave's method (Hargreaves and Allen, 2003). Note that effective rainfall can be either positive (i.e. moisture input from rainfall exceeds moisture loss due to evapotranspiration causing an increase in soil moisture) or negative (i.e. moisture input from rainfall is less

than moisture loss from evapotranspiration resulting in drying of the near surface).

Piezometric levels

Stand-pipe and water level loggers (Solinst Levellogger Junior Edge) were installed on each earthflow and recorded groundwater level from September 2009. A borehole was advanced to depths of 2.85 m and 2.8 m on the western and eastern lobes, respectively. These depths were chosen in order to place the active zone of the piezometers in the vicinity of the depth to predicted shear surfaces, which were determined using cone penetration testing (CPTU) downhole tool measurements (Gunn *et al.*, 2013). A 19 mm uPVC pipe, fitted with a 0.9 m slotted, porous piezometer tip was installed in each stand-pipe (see Figure 1 for location). Each hole was backfilled with clean sand to 1.95 m and 1.75 m below ground for the western and eastern piezometer, respectively, forming an active zone that allows for monitoring of the pore water pressure in the vicinity of the slip surface (located at 1.6 m depth on the eastern lobe). The remainder of the borehole was backfilled using bentonite granules to ensure sealing. Since the active zones of the piezometers are in close proximity to the shear surface (< 0.35 m), the measured pore water pressures are indicative for the conditions at the shear surface. The piezometer is located at a depth in the standpipe corresponding to the depth of the deepest periodically active slip surface. Meanwhile, the depth of the most active slip surface (~ 0.8 m depth below ground level in the eastern earthflow) is annotated along with piezometry in Figures 4 and 6.

Ground movement

Ground movement and estimates of landslide activity were derived from GPS measurements of benchmarks, as described in the electrode position interpolation section (see also Uhlemann *et al.*, 2015a, b), and from tilt meter records (Uhlemann *et al.*, 2015b and 2017). These records provide evidence of landslide activation and very slight slope displacements, which began early to mid-July 2012.

Results

Overview

To our knowledge, the application of temperature-corrected electrical resistance measurements to observe the hydrogeological precursors to shallow landslide activation has not previously been reported in the literature. Therefore, the content of the results section aims to provide a complete analysis of the processes taking place within the shallow subsurface throughout the monitoring period. The results section is divided into four sections; the first, presents general geophysical observations of general hillslope processes, while the second and third sections focus on earthflow activation processes at both high-temporal and high-spatial resolutions, respectively. The landslide system is divided into several regions

based on the hydrogeological behaviour. These regions were formulated through integration of monitoring datasets.

General monitoring results: 2008–2013

Baseline data on landslide movement and environmental conditions were established in this period (Figure 4). Table 2 contains a summary of general hillslope and earthflow monitoring observations. Statistical analysis of piezometric levels and TC-res data reveal strong negative correlation coefficient of -0.65 (Schumann, 1998), while a P -value of <0.001 confirms that there is significant correlation between the two datasets. Note that the lag between the piezometric and resistivity data was taken to be zero since observed lags in similar studies have only been significant on timescales of hours to days (Chambers *et al.*, 2015). The results from the four measurement locations respond to 'wet' and 'dry' periods to different degrees.

Table 2. Summary of general monitoring results as displayed in Figure 4

Environmental inputs	Electrical resistance response (TC-res)	Interpreted ground response
<p>Periods of higher than average rainfall (positive effective rainfall), e.g. October 2009 to April 2010. Results in rising piezometric levels.</p>	<p>TC-resistance values fall, e.g. resistance ratio at Measurement Location 1 (ML1) reduces from 1.35 to 1.15.</p>	<p>Increase moisture content in the subsurface. Soil moisture accumulation manifests as both water level rise and very shallow soil moisture accumulation.</p>
<p>Periods of lower than average rainfall (negative effective rainfall), e.g. May 2010 to September 2010. Piezometric levels during these periods lowered by ~0.6 m (from 78.0 m ~77.4 m AoD).</p>	<p>TC-resistance values rise. e.g. resistance ratio at ML1 rises from 1.2 to 1.5.</p>	<p>Decrease moisture content in the subsurface. Soil moisture depletion manifest as both water table fall and drying of soil in the very shallow subsurface.</p>
<p>An intense period of rainfall (positive effective rainfall) during and after a period of low rainfall (negative effective rainfall). e.g. September 2010. Rapid</p>	<p>TC-res ratios fall rapidly. e.g. resistance ratio at ML1 falls from 1.5 to 1.25.</p>	<p>Annealing of desiccation cracking in response to rainfall, as soil moisture content increases in very shallow subsurface. Some phreatic water reaches the water table.</p>

Environmental inputs	Electrical resistance response (TC-res)	Interpreted ground response
<p>piezometric level rise concurrent with rainfall event.</p>		
<p>Minor, low intensity rainfall event, as occurred June to July 2011 and do not create a piezometric level rise.</p>	<p>Small rises and falls in resistance ratio between 1.4 to 1.3.</p>	<p>Soil moisture accumulation in the very shallow subsurface occurring. Insufficient quantity of rain water to reach the water table.</p>
<p>Full range of seasonal weather.</p>	<p>Measurement location (ML) 1 results reveal a greater temperature-corrected resistance ratio range (0.6) than the other three measurement locations, with ML4 showing the most subtle variation (0.25).</p>	<p>The thinnest region of the earthflows (nearest the toe) respond more extremely to environmental conditions than regions where the earthflow is thicker (closer to the main landslide body) and composed of several flows.</p>
<p>Earthflow activation caused by high and sustained piezometric levels.</p>	<p>November 2012 until the end of the monitoring period, the resistances recorded using the four measurement locations diverge markedly, with</p>	<p>This occurs during a period of earthflow activity and is attributed to the resulting displacement of individual electrodes, fissuring in the near surface, and localised</p>

Environmental inputs	Electrical resistance response (TC-res)	Interpreted ground response
	<p>ML1 and ML2 displaying extreme increases and decreases in resistance respectively.</p> <p>It should be noted that this trend is not observed in the 2008 activation (within Figure 4) because a separate earthflow lobe was active during this activation event.</p>	<p>accumulations of moisture - all of which would influence electrical resistance measurements.</p>

Two wetter periods of substantially longer duration exist during the entirety of 2008 and only three short periods of negative effective rainfall occurred between July 2011 and March 2013 (see Figures 4 and 6). The two years where landslide activations occurred during the monitoring period took place during years with higher than average annual rainfall (751 mm/year) (Figure 5). Both of these prolonged wet periods are associated with earthflow activation events with the latter being discussed in more detail later. Earthflow deposits activated during these prolonged wet periods, between July 2008 and April 2009 and August 2012 and February 2013.

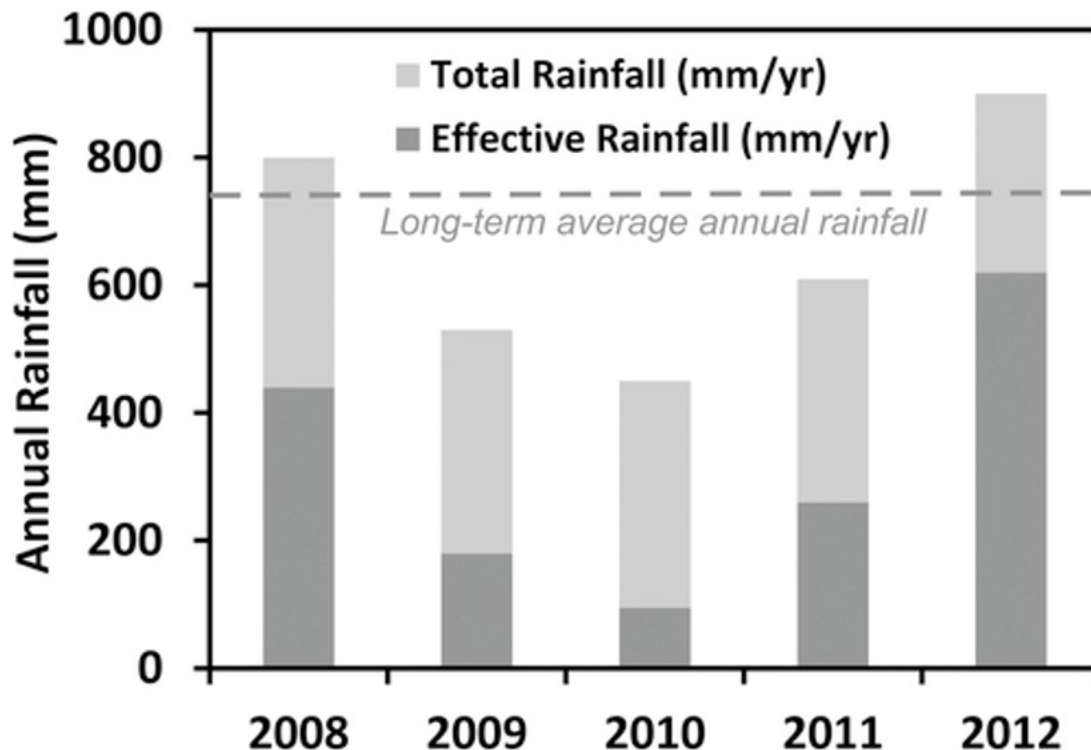


Figure 5

Total and effective annual rainfall throughout the landslide monitoring period. Rainfall data is from the rain gauge installed at the test site. The dashed line shows the long-term (30 year) average annual rainfall in the area of the test site.

Pre-reactivation and reactivation monitoring: 2011-2013

Temperature corrected resistance results in the 14 months leading to earthflow activation are presented in Figure 6 and reveal several additional trends associated with progressive landslide activation processes. July 2011 was preceded by a three month period of negative effective rainfall and so is characterised by low piezometric levels and some of the highest TC-resistances recorded during the monitoring period (ML1 has resistance ratios close to 1.4). July and August 2011 see resistances fluctuate yet remain high, in response to two periods of rainfall. These rainfall events are not sufficient to raise the piezometric level and so the piezometer remains constant at

77.6 m AoD. Piezometric levels rise slightly at the end of August 2011 in response to rainfall at a time when the ALERT array was not fully functional.

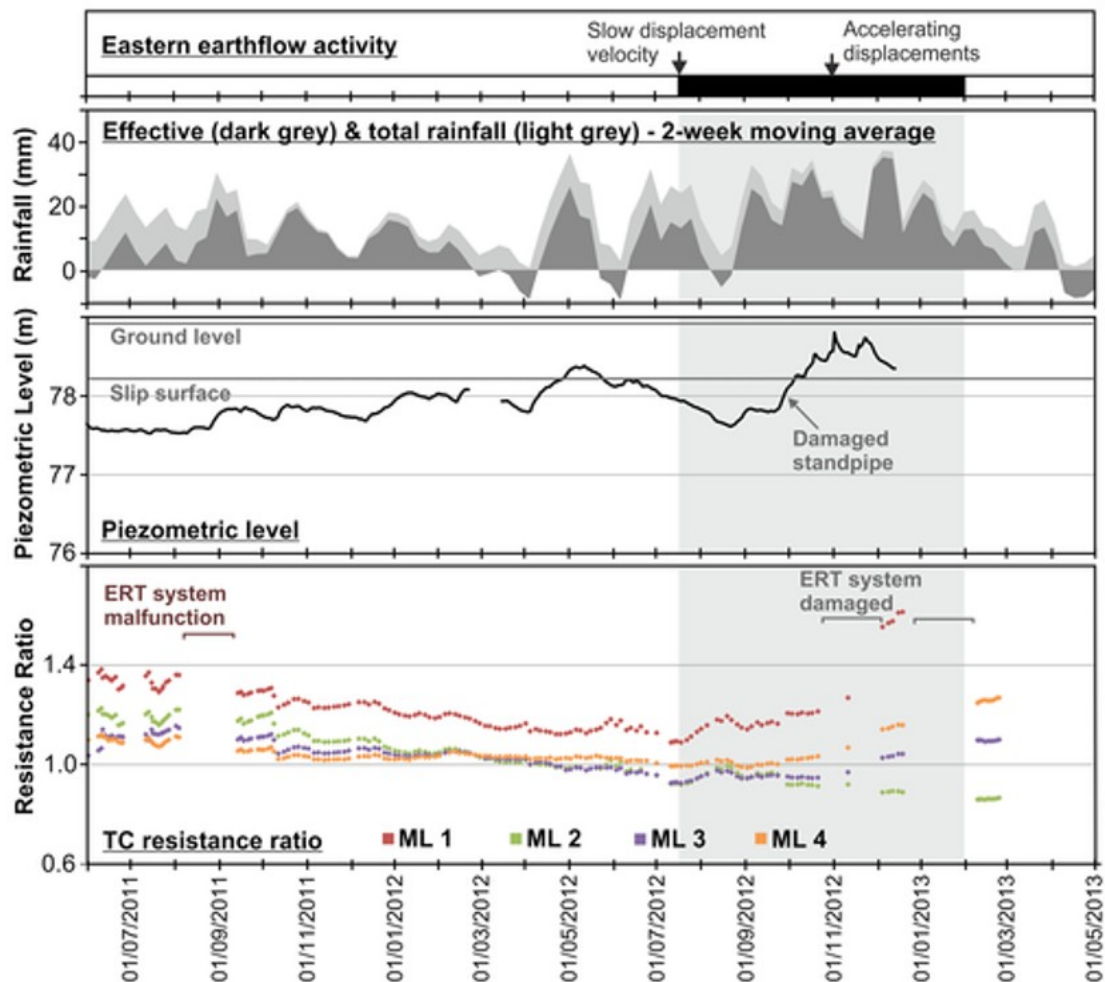


Figure 6

Goelectrical monitoring of landslide deposit results for the 14 months leading to earthflow activation (July 2011–March 2013). Subsurface ground conditions and environmental inputs are also presented in the form of piezometry and rainfall, respectively. NB: Piezometry and resistance data not present during several periods due to technical issues.

Between August 2011 and February 2012 three periods of prolonged positive effective rainfall occurred, ranging between 21 mm and 17 mm of weekly rolling averaged rainfall. These three periods result in a 0.6 m rise in piezometric level and occurs in a stepped manner. During this 7 month time-frame TC-resistances across all four earthflow measurement locations markedly decrease. ML1 exhibits the greatest decrease from 1.35 to 1.15, with the other three measurement locations displaying less pronounced decreases of between 0.05 and 0.15.

March 2012 is a relatively dry month as it experienced only negative effective rainfall, and was accompanied by associated piezometric level falls and TC-resistances either slightly rise (ML1, 0.1 rise) or remain constant. The

next six weeks (April to early May 2012) saw a rapid piezometric level rise from 77.8 m to 78.4 m AoD. TC-resistance for all four earthflow measurement locations either remain constant or decrease slightly during this time and could be indicative of the imaged slope material nearing saturation. The second half of May experiences negative effective rainfall and the piezometric level fall causes ML1 resistance ratios to increase by 0.15. The other three measurement locations again either remain relatively constant or reduce very slightly.

Between June and mid-August 2012, piezometric levels fall at a time when relatively high rainfall is recorded. TC resistances during this period initially decrease during June but then increase during the latter half of July 2012. Earthflows reactivate at a time when piezometric levels are falling and TC resistance values are at a 24 month minimum. Once movement is initiated, earthflows remain active until February 2013, a duration of just over six months. During this active period rainfall is at its most intense (the three highest peaks occur during this period).

One month after earthflow reactivation piezometric levels begin to rise once again and TC resistances reduce and level off at between 0.9 (ML2 and ML3) and 1.15 (ML1). TC resistance values begin to jump (diverge), either more positive or negative, from October 2013 until the end of the monitoring period. The earthflow-installed piezometer became trapped in the standpipe during this period, hinting at substantial earthflow displacement. Piezometric levels reach their highest levels during the active earthflow period (November 2012), and are coincident with substantial TC resistance divergence.

Pre-reactivation and reactivation monitoring maps: 2011-2013

The spatial variation of temperature corrected resistance is presented as a series of 12 time-lapse resistance maps (which show TC resistance change relative to a baseline) extending over the 14 month period preceding earthflow reactivation (Figure 7). The baseline is an average of resistance measurements made during 2010, a period when the landslide was inactive. Each map represents a snapshot in time, and it is therefore more difficult to identify trends in the data compared with the high frequency resistance ratio time-series given in Figures 4 and 6; nevertheless, temporal and spatial patterns can be observed. First, the earthflow region and the SSF towards the base of the slope show significantly more variability in response to rainfall than the upper regions of the slope - perhaps indicating higher infiltration rates towards the base of the slope due to fissuring and, in the case of the SSF, coarser material and hence higher permeability. Second, around the time of earthflow reactivation the lower earthflow regions of the landslide show a very marked decrease in resistance (i.e. increase in moisture) to levels lower than at any time in the preceding 12 months. High levels of spatial variability are observed in the earthflow regions, which

reflects ground movement resulting in fissuring and localised accumulation and drainage of moisture.

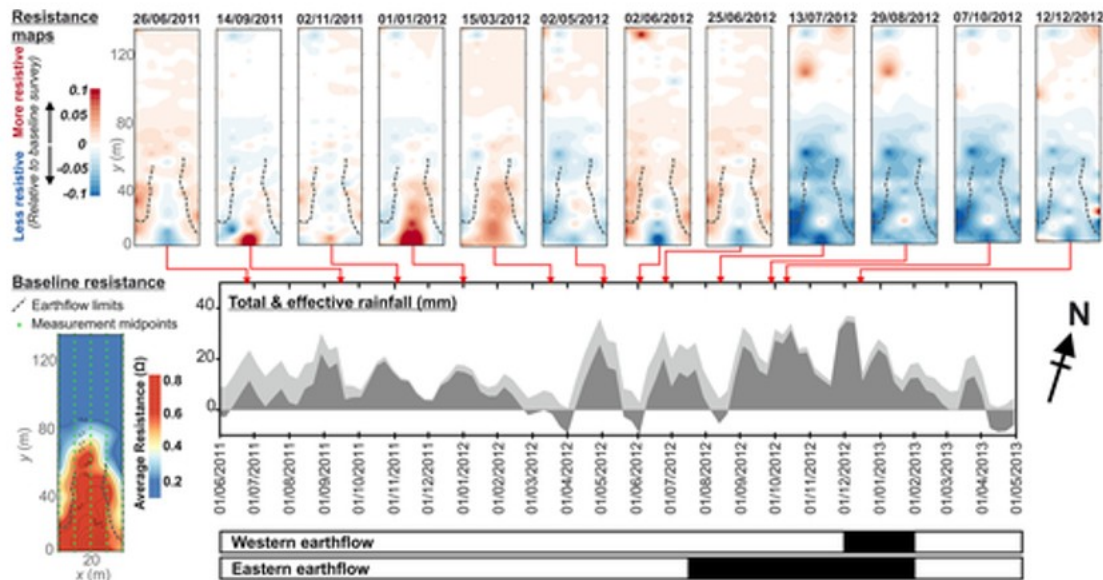


Figure 7

Temperature corrected transfer resistance difference maps (top) between June 2011 and December 2012, showing difference in resistance relative to the baseline. The baseline resistance map (bottom right) is an average of all the resistance measurements throughout 2010. Rainfall and periods of earthflow activity (bottom left).

Pre-reactivation and reactivation monitoring by zones: 2011–2013

The landslide system is divided into zones based on their electrical responses to environmental inputs. The landslide zones are shown on Figure 8, and Table 2 is a summary of interpreted hillslope hydrogeological behaviours. In brief, Zones 1, 2 and 3 are defined as the Backscarp, Head and Sag Pond, and Upper Body, respectively. These three zones display relatively small changes in resistance over the period, which is possibly due to the low permeability clay soil and a relative lack of fissuring resulting in more consistent moisture retention. No significant decrease in resistance is observed in the months preceding landslide activation, although a small drop in resistance and greater variability accompanies the period of landslide movement towards the end of 2012. Zone 4 is defined as the Lower Body and Flow Lobes, and displays a steady drop in resistance in the months preceding landslide activation, which is in accordance with the resistance measurements shown in Figure 6. This is the most active region of the landslide system, with the greatest degree of fissuring. Zone 5 is defined as Between Flow Lobes and is a stable region of well drained SSF.

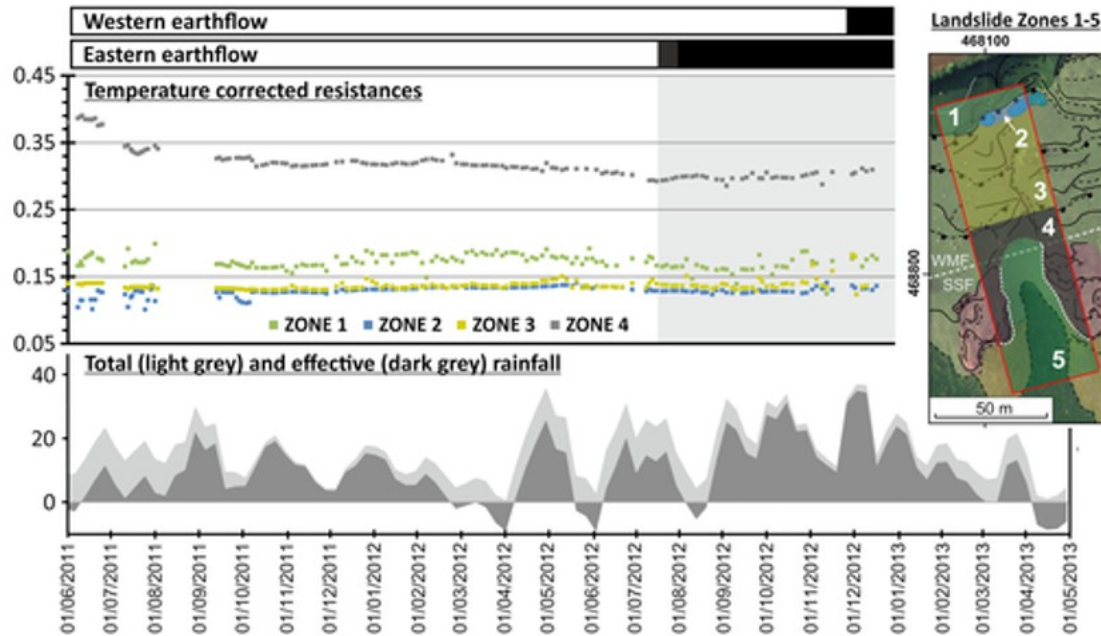


Figure 8

Diagram showing locations of individual landslide system and hillslope zones. BGS © NERC. Contains Ordnance Survey data © Crown Copyright and database rights 2016.

Discussion

Processing of raw resistance measurements

Plotting of raw transfer resistance monitoring data – without any form of processing – revealed that subtle resistance changes are masked by seasonal air temperature variations which propagate into the subsurface. This is a significant limitation for the monitoring and investigation of shallow landslides (<5 m). It will have less impact on deeper landslide systems in temperate climates. The sinusoidal nature of transfer resistance variation in response to air temperature variation acts to reduce resistance in the summer months when air temperature is higher than the annual average temperature and increases resistance in the winter months when air temperature is lower than the annual average.

Temperature correcting raw resistance monitoring results using the method proposed by Hayley *et al.* (2010) makes interpretation of resistance results for shallow landslides much simpler as one major external process which affects resistance seasonally has been modelled and removed. By altering the procedure outlined by Hayley *et al.* (2010) to model a correction ratio for every transfer resistance measurement, as opposed to modelling a single correction factor and applying it to all transfer resistances, the method was adapted to be more applicable to monitoring landslides, because measurement electrode geometries change when landslides activate.

Subsurface environmental conditions

The main trends observed in temperature corrected resistance data include: TC resistance ratio highs during periods of low piezometric levels, and conversely, resistance ratio lows when piezometer levels are high. The eastern earthflow resistances reveal that some small rainfall events are not identified by piezometry but are responsible for small changes in resistance and, are attributed to the transfer resistances being sensitive to shallow moisture content and that piezometer observations only provide point data in the landslide system.

Resistances measured on the upper body of the landslide change more slowly in response to negative effective rainfall (i.e. drying). This is likely to be the result of fewer tension cracks within the slump section of the landslide, and them rapidly annealing after rainfall. Given that the main scarp of the slump transmits surface runoff into the earthflow systems the presence or absence of cracking here influences reactivation strongly. The upper body of the slumped region (Figure 1, Figure 8 - Zone 3, Figure 9) dips less steeply than earthflow regions, precipitation therefore has the time to penetrate the subsurface, and runoff only occurs after crack annealing has taken place. This small resistance variation observed at this region is attributed to the soil moisture varying very little throughout the year. Its small resistance variation and lack of rainfall infiltration flow pathways potentially indicates that the slump region of the landslide holds on to its moisture and doesn't freely release it like the heavily cracked earthflow region.

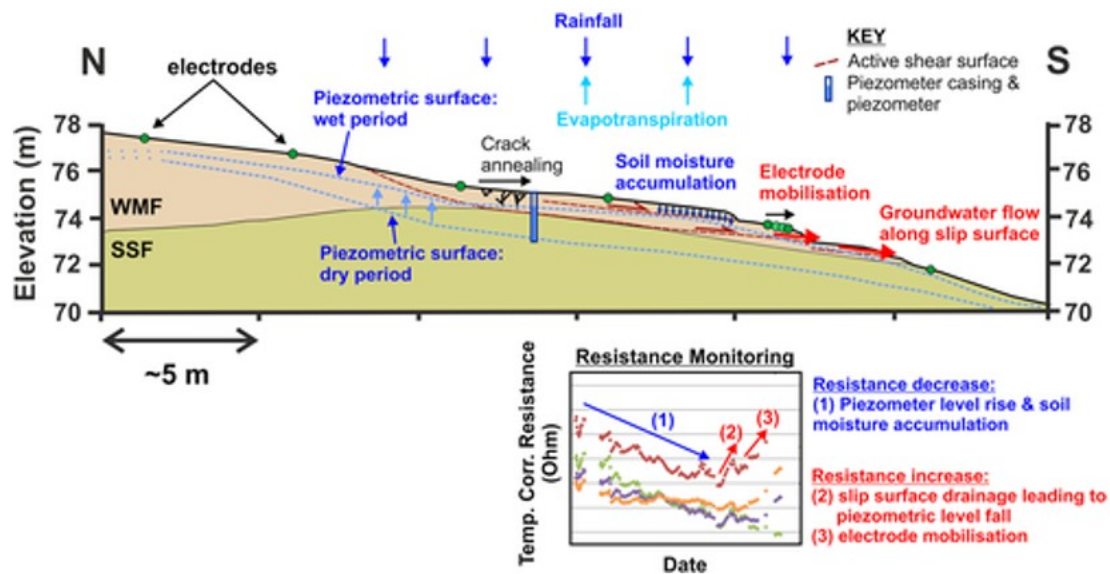


Figure 9

Conceptual ground and resistance models showing subsurface hydrogeological precursory behaviour to earthflow activation.

Resistance monitoring results were compared with piezometer measurements of the eastern earthflow region. Correlation coefficients between the two datasets suggest a negative correlation (-0.65) between

piezometry and electrical resistance response. Therefore, as piezometric level rises due to rainfall infiltration the electrical resistances generally decrease, which is similar to the behaviour reported by Lebourg *et al.* (2010) in a short-term landslide monitoring study in sandy clay materials. However, it should be noted there are deviations from this pattern in the data that have not previously been observed; for example in the month preceding activation piezometric levels show a consistent drop (albeit from a three year peak), whereas over the same period a drop in resistance is observed followed by a period of increase. This is discussed further in the following section.

Pervasive and deep cracking presents an impediment to electrical current flow, and therefore results in resistance increases in the vicinity of cracking. This trend of more elaborate resistance responses to environmental factors is attributed to thin earthflow regions being more susceptible to pervasive desiccation during dry summer months. They are more susceptible because the shear surfaces between individual flows act both as a conduit for water drainage, assisting flow through and out to underlying formation, and as an aid to joining up desiccation cracks, further encouraging their development. The opening of cracks within the silty clay dominated earthflows is thought to become more effective as the dry spell progresses, as cracks open up the ground to further drying and causes resistances to continue increasing. Resistance values reach a summer peak at around August/September associated with desiccation.

Desiccated earthflow toes of Zone 4 (Figure 8), composed of a series of overlapping and overriding thin landslide deposits, may permit more fluid to enter the subsurface when compared with less desiccated thick successions of WMF (Figure 8 - Zone 3). This is due to desiccation cracks being conduits for fluid to enter the subsurface. Furthermore, these cracked earthflow regions retain very little rainwater and as a result resistances in these regions rise and fall sharply.

These observations accord with those of Bièvre *et al.* (2012) in that the geophysical signatures of fissure dynamics are similar and indicate that preferential flow is occurring; however, the longer term spatial monitoring presented here has shown a greater range of fissure behaviour (crack formation and annealing) and more variable drainage associated with longer term spatial monitoring over many seasonal cycles in a more complex landslide system.

Earthflow reactivation mechanisms

The sensitivity of the resistance monitoring system to soil moisture accumulation and piezometric level variation highlights an interesting process taking place in the months preceding earthflow reactivation (Figures 6 and 9). The system successfully identified the fall in piezometric levels up to June 2012 (Figure 6), which manifested as an increase in resistance up to this point. However, as described in the previous section, the two measures

deviated from one another shortly in advance of landslide reactivation; despite significant rainfall, piezometric levels dropped, while resistance decreased. The drop in piezometric levels leading up to landslide reactivation was unexpected, as increased pore pressures are widely recognised as a key driver of landsliding (Iverson and Major, 1987; Malet *et al.*, 2005; Handwerger *et al.*, 2013). However, the observed decreases in measured resistances (or increases in moisture content) to a 24 month low are consistent with landslide reactivation. The deviations between the two measures are likely to be related to subsurface heterogeneity and sampling volume; the resistance measurements are sampling a significant volume of ground below a 14.25 m array, whereas the piezometer is sampling a much smaller volume of ground, and is, therefore, likely to be more effected by very local heterogeneities and fissuring. Given that the piezometer is recording perched water levels within highly disturbed (and potentially mobile) earthflow material above permeable bedrock (Figures 2 and 9), it is probable that local fissure flow and drainage along failure planes caused the anomalous declining water levels observed from June to August 2012. This is supported by Gunn *et al.* (2013), who reported water and washed out fine material emerging from the slip surfaces at the earthflow toes during periods of activation. Likewise this is also consistent with observations on other slow moving landslide where the role of fissuring, including the dynamic opening and closing of flow pathways, is seen to significantly influence ground water movement (Van Asch *et al.*, 1999; Bièvre *et al.*, 2012; Krzeminska *et al.*, 2013).

By September 2012 continuing rainfall resulted in increased piezometric levels once again as resistances briefly fall during September and October 2012. From November 2012 piezometric levels are high (approaching ground level) and result in larger, deeper, more rapid earthflows activating. November onwards marks a time when electrodes are mobilising and is represented on temperature corrected plots as divergence and jumps in resistance values.

It should be reiterated at this point that the principal mechanism controlling movement of slow moving earthflows involves fluctuating pore pressures associated with changing groundwater levels. Increasing deformation rates generally follow a rise in these water levels that results in an increase in pore pressures, a concomitant loss of effective stress and thus a lower shearing resistance in these earthflows, particularly along bounding failure surfaces (Terzaghi, 1950). When associated with transitions from partial to full saturation, instability is compounded by increased loading of the landslide mass (Varnes, 1978).

Summary of findings

Analysis of the results of this investigation reveals several new contributions to the understanding of landslide hydrogeological processes and resistance monitoring. These are stated in Table 3.

Table 3. Summary of the results of temperature-corrected resistance monitoring of an intermittently active complex landslide system

	Hydrogeological landslide processes
1	Significant seasonal and spatial variations in subsurface response to rainfall input can be seen across the different zones of the landslide, including in the lead-up to earthflow activation.
2	The intensity and distribution of desiccation cracking (and conversely, annealing) exerts a significant influence on slope hydrogeological dynamics.
3	The process of shallow slow-moving earthflow activation may be more complex than initially thought. Resistance monitoring identified the presence of fissure flow along the landslide slip surfaces.
4	Temperature-corrected resistance monitoring is sensitive to a key shallow earthflow activation mechanism, i.e. the rise in pore water pressure as a result of high and sustained piezometric levels.
	Temperature-corrected resistance monitoring
1	Temperature corrected resistance measurements are sensitive to both shallow rainfall driven moisture dynamics and piezometric level changes.
2	Upon landslide activation, electrode displacement causes divergence or convergence of resistance values.
3	Shallow resistance measurements are highly sensitive to seasonal temperature variations. These temperature variations act to mask subtle

Hydrogeological landslide processes

moisture content related resistance changes.

Conclusions

When applied to observe landslide processes, time-lapse electrical resistance makes use of its sensitivity to variation in moisture content in the subsurface. Resistance monitoring informs about the manner in which the slope responds to rainfall infiltration and soil moisture accumulation.

Landslides respond to changing ground conditions, i.e. rising piezometric level or soil moisture content reaching plastic limits, which can bring about a change in internal physical properties, such as soil strength.

This investigation provides the longest term analysis of electrical resistance data for landslide monitoring that we are aware of in the literature, and extends the pioneering resistance monitoring work of Lebourg *et al.* (2010) and Palis *et al.* (2017) by providing spatial data from a grid of electrodes (rather than linear arrays) and detailed consideration of both the influence of temperature and electrode motion.

Compensating for temperature effects and accounting for electrode movements was shown to be essential in interpreting the geophysical events, as both of these processes can mask the moisture driven processes that the resistance monitoring system is designed to observe.

The spatial element of the monitoring described here was also shown to be highly significant. Landslides invariably display heterogeneous ground conditions with complex hydraulic processes, which can be difficult to characterise using point sampling or linear monitoring arrays. The spatial geophysical monitoring presented here provides information on how the landslide system as a whole responded to fissuring events, rainfall infiltration and changes in piezometric levels. This greatly assisted in identifying and characterising the different zones within the system (e.g. Figure 8 and Table 4).

Table 4. Landslide system and hillslope zones and associated electrical resistance and interpreted ground response. The locations of the landslide zones are shown in Figure 8

	Landslide zone	Electrical resistance response	Interpreted ground response leading to earthflow activation
1	Backscarp	Resistances display only small variations. However, resistances are slightly lower than baseline August to January and slightly higher than baseline between February and July.	Small moisture content variations due to soil moisture retention and lack of considerable fissuring. Potential supply of moisture from the Dogger Formation, a minor aquifer in the area.
2	Head & Sag Pond	Resistances are equal to or slightly higher than baseline.	Region retains soil moisture throughout period due to slight back-tilt of beds, shading by backscarp and reed-beds.
3	Upper Body	Small resistance changes throughout the year. July to February is equal to baseline. March to June is higher than baseline.	Water table level not greatly variable in lead up to earthflow activation. Little evidence for soil surficial cracking, any cracks present are quickly annealed following rainfall.
4	Lower Body & Flow Lobes	Response is more sudden and extreme. Rapid Resistance Change; uniformly higher 06/2011 and lower 05/2012.	Flow lobes are composed of a series of 0.5–1.0 m earthflow deposits. These permit easy fluid through-flow during wet periods and cracking when dry. Ground responds rapidly to negative

Landslide zone	Electrical resistance response	Interpreted ground response leading to earthflow activation
5	Between Flow Lobes	Markedly lower resistances than baseline from 05/2012 onwards and during the three month period preceding activation. Resistances remain low
	<p>Winter 2011 (09/2011-01/2012) variable response, small regions of higher and lower resistance. When Upper Body of landslide system is near equal to resistance baseline the lower body and flow lobes show lower resistances.</p> <p>Lowest resistances measured occur during the month preceding earthflow activation. Very low resistances at earthflow toes.</p>	<p>effective rainfall events by desiccation and lowering of perched water table within WMF.</p> <p>Runoff occurring from Upper Body to penetrate the Lower Body and Flow Lobes.</p> <p>Rising piezometric level within earthflow zone during the lead up to earthflow activation. Pore pressures high enough to permit earthflow activation. Groudwater flow occurring along slip surfaces and out at earthflow toe.</p> <p>Regional water table within Staithes Sandstone Formation rising in response to positive effective rainfall.</p>

Landslide zone	Electrical resistance response	Interpreted ground response leading to earthflow activation
while earthflows are active.		

Crucially, this study confirms the suitability of spatially distributed, temperature corrected resistance monitoring for landslide early warning by analysing multi-year variations in geophysical properties, which have permitted us to identify precursors to failure events. The sensitivity of this approach to changes in subsurface water distribution, and piezometric levels in particular, is key to its success because it can therefore observe the principal activation mechanism of slow-moving shallow earthflows, i.e. the reduction in effective normal stress due to increasing pore water pressures.

The capability of observing increased moisture content with time provides a powerful tool to reveal hill slope hydrogeology, infiltration and landslide activation mechanisms. The technique highlights great potential to provide early warning of imminent slope failure when combined with additional a priori geotechnical data. Specifically, it provides a simple, fast, and non-invasive means of using resistance time-series data in order to monitor the moisture dynamics of landslide prone slopes thereby providing early warning of failure events.

Acknowledgements

We would like to extend our gratitude to Josie Gibson (the Hollin Hill landowner) for her support and cooperation in the research. This paper is published with the permission of the Executive Director of the British Geological Survey (NERC).

References

- Bièvre G, Jongmans D, Winiarski T, Zumbo V. 2012. Application of geophysical measurements for assessing the role of fissures in water infiltration within a clay landslide (Trièves area, French Alps). *Hydrological Processes* 26: 2128– 2142. <https://doi.org/10.1002/hyp.7986>.
- Brunet P, Clement R, Bouvier C. 2010. Monitoring soil water content and deficit using electrical resistivity tomography (ERT) – a case study in the Cevennes area, France. *Journal of Hydrology* 380: 146– 153.
- Cannon J. 1984. The one-dimensional heat equation. In *Encyclopedia of Mathematics and Its Applications* 23, 1st edn. Addison-Wesley Publishing Company/Cambridge University Press. ISBN:978-0-521-30243-2.
- Chambers JE, Wilkinson PB, Kuras O, Ford JR, Gunn DA, Meldrum PI, Pennington CVL, Weller AL, Hobbs PRN, Ogilvy RD. 2011. Three-dimensional geophysical anatomy of an active landslide in Lias Group mudrocks, Cleveland Basin, UK. *Geomorphology* 125: 472– 484.
- Chambers JE, Gunn DA, Wilkinson PB, Meldrum PI, Haslam E, Holyoake S, Kirkham M, Kuras O, Merritt A, Wragg J. 2014. 4D Electrical Resistivity Tomography monitoring of soil moisture dynamics in an operational railway embankment. *Near Surface Geophysics* 12: 61– 72.
- Chambers JE, Meldrum PI, Wilkinson PB, Ward W, Jackson C, Matthews B, Joel P, Kuras O, Bai L, Uhlemann S, Gunn D. 2015. Spatial monitoring of

groundwater drawdown and rebound associated with quarry dewatering using automated time-lapse electrical resistivity tomography and distribution guided clustering. *Engineering Geology* 193: 412- 420.

Cruden DM, Varnes DJ. 1996. Landslide types and processes. In *Special Report 247: Landslides: Investigation and Mitigation*. Transportation Research Board, Washington DC.

Dijkstra TA, Jenkins GO, Gunn DA, Dashwood C, Dankers R, Dixon N, Petley DN, Gibson AD, Winter MG. 2014. Landslides and Climate Change in the United Kingdom. Joint Technical Committee on Natural Slopes and Landslides (JTC 1) TR3 Report.

Dijkstra TA, Dixon N. 2010. Climate change and slope stability: challenges and approaches. *Quarterly Journal of Engineering Geology and Hydrogeology* 43(4): 371- 385.

Dixon N, Spriggs MP, Smith A, Meldrum P, Haslam E. 2014. Quantification of reactivated landslide behaviour using acoustic emission monitoring. *Landslides* 12: 549- 560 <https://doi.org/10.1007/s10346-014-0491-z>.

Foster C, Jenkins GO, Gibson AD. 2007. Landslides and mass movement processes and their distribution in the York District (Sheet 63). British Geological Survey Open Report, OR/07/004. 49.

Friedel S, Thielen A, Springman SM. 2006. Investigation of a slope endangered by rainfall-induced landslides using 3D resistivity tomography and geotechnical testing. *Journal of Applied Geophysics* 60(2): 100- 114.

Gance J, Malet JP, Supper R, Sailhac P, Ottowitz D, Jochum B. 2016. Permanent electrical resistivity measurements for monitoring water circulation in clayey landslides. *Journal of Applied Geophysics* 126: 98- 115. <https://doi.org/10.1016/j.jappgeo.2016.01.011>.

Gunn DA, Chambers JE, Hobbs P, Ford J, Wilkinson PB, Jenkins G. 2013. Rapid observations to guide the design of systems for long-term monitoring of a complex landslide in the Upper Lias, North Yorkshire. *Quarterly Journal of Engineering Geology and Hydrogeology* 46: 323- 336.

Handwerger AL, Roering JJ, Schmidt DA. 2013. Controls on the seasonal deformation of slow-moving landslide. *Earth and Planetary Science Letter* 377-378: 239- 247.

Hargreaves GH, Allen RG. 2003. History and evaluation of Hargreaves evapotranspiration equation. *Journal of Irrigation and Drainage Engineering* 129(1): 53- 63.

Hayley K, Bentley LR, Gharibi M, Nightingale M. 2007. Low temperature dependence of electrical resistivity: implications for near surface geophysical monitoring. *Geophysical Research Letters* 34: L18402.

- Hayley K, Bentley LR, Pidlisecky A. 2010. Compensating for temperature variations in time-lapse electrical resistivity difference imaging. *Geophysics* 75(4): WA51- WA59.
- Ingeman-Nielsen T, Baumgartner F. 2006. CR1Dmod: a Matlab program to model 1D complex resistivity effects in electrical and EM surveys. *Computers and Geosciences* 32: 1411- 1419.
- Intrieri E, Gigli G, Casagli N, Nadim F. 2013. Brief communication 'Landslide Early Warning System: toolbox and general concepts'. *Natural Hazards Earth Systems Science* 13: 85- 90.
- Iverson RM, Major JJ. 1987. Rainfall, groundwater-flow, and seasonal movement at Minor Creek landslide, northwestern California - physical interpretation of empirical relations. *Geological Society of America Bulletin* 99(4): 579- 594.
- Jomard H, Lebourg T, Tric E. 2007. Identification of the gravitational discontinuity in weathered gneiss by geophysical survey: La Clapiere landslide (France). *Journal of Applied Geophysics* 62: 47- 57.
- Jones DKC, Lee EM. 1994. Landsliding in Great Britain. Department of the Environment, London, 390.
- Krzeminska DM, Bogaard TA, Malet JP, van Beek LPH. 2013. A model of hydrological and mechanical feedbacks of preferential fissure flow in a slow-moving landslide. *Hydrology and Earth System Sciences* 17(3): 947- 959.
- Lebourg T, Binet S, Tric E, Jomard H, El Bedoui S. 2005. Geophysical survey to estimate the 3D sliding surface and the 4D evolution of the water pressure on part of a deep seated landslide. *Terra Nova* 17(5): 399- 406.
- Lebourg T, Hernandez M, Zerathe S, El Bedoui S, Jomard H, Fresia B. 2010. Landslides triggered factors analysed by time lapse electrical survey and multidimensional statistical approach. *Engineering Geology* 114(3-4): 238- 250.
- Lehmann P, Gambazzi F, Suski B, Baron L, Askarinejad A, Springman SM, Holliger K, Or D. 2013. Evolution of soil wetting patterns preceding a hydrologically induced landslide inferred from electrical resistivity survey and point measurements of volumetric water content and pore water pressure. *Water Resources Research* 49(12): 7992- 8004.
- Lourenco S, Gallipoli D, Toll D, Augarde C, Evans F. 2011. A new procedure for the determination of soil-water retention curves by continuous drying using high-suction tensiometers. *Canadian Geotechnical Journal* 48: 327- 335.
- Loveridge FA, Spink TW, O'Brien AS, Briggs KM, Butcher D. 2010. The impact of climate and climate change on infrastructure slopes, with particular reference to southern England. *Quarterly Journal of Engineering Geology and*

Hydrogeology 43(461-472): 1470- 9236/10 <https://doi.org/10.1144/1470-9236/09-050>.

Malet JP, van Asch TWJ, van Beek R, Maquaire O. 2005. Forecasting the behaviour of complex landslides with a spatially distributed hydrological model. *Natural Hazards and Earth System Sciences* 5(1): 71- 85.

Merritt AJ, Chambers JE, Murphy W, Wilkinson PB, West LJ, Gunn DA, Meldrum PI, Kirkham M, Dixon N. 2014. 3D ground model development for an active landslide in Lias mudrocks using geophysical, remote sensing and geotechnical methods. *Landslides* 11: 537- 550
<https://doi.org/10.1007/s10346-013-0409-1>.

Merritt AJ, Chambers JE, Wilkinson PB, West LJ, Murphy W, Gunn D, Uhlemann S. 2016. Measurement and modelling of moisture - electrical resistivity relationship of fine-grained unsaturated soils and electrical anisotropy. *Journal of Applied Geophysics* 124: 155- 165
<https://doi.org/10.1016/j.jappgeo.2015.11.005>.

Moore R, Turner MD, Palmer M, Carey JM. 2007. The Ventnor Undercliff: a new ground model and implications for climate induced landslide behaviour and risk. In *Landslides and Climate Change - Challenges and Solutions*, R McInnes, J Jakeways, H Fairbank, E Mathie (eds), Proceedings of the International Conference on Landslides and Climate Change. Ventnor: Isle of Wight; 365- 376.

O'Brien AS, Scott JM, Loveridge F. 2007. Influence of Climate and Vegetation on Railway Embankments. Proceedings XIV European Conference on Soil Mechanics and Geotechnical Engineering, Madrid, September 2007.

Palis E, Lebourg T, Tric E, Malet J, Vidal M. 2017. Long-term monitoring of a large deep-seated landslide (La Clapiere, South-East French Alps): initial study. *Landslides* 14: 155- 170 <https://doi.org/10.1007/s10346-016-0705-7>.

Papa MN, Medina V, Ciervo F, Bateman A. 2013. Derivation of critical rainfall thresholds for shallow landslides as a tool for debris flow early warning systems. *Hydrology and Earth System Sciences* 17(10): 4095- 4107.

Perrone A, Lapenna V, Piscitelli S. 2014. Electrical resistivity tomography technique for landslide investigation: a review. *Earth Science Reviews* 135: 65- 82.

Reid ME, LaHusen RG, Baum RL, Kean JW, Schulz WH, Highland LM. 2012. Real-time monitoring of landslides. US Geological Survey Fact Sheet 2012-3008, 4.

Schumann AH. 1998. Correlation Coefficient. *Encyclopedia of Hydrology and Lakes* 145. https://doi.org/10.1007/1-4020-4497-6_47.

Segoni S, Battistini A, Rossi G, Rosi A, Lagomarsino D, Catani F, Moretti S, Casagli N. 2015. Technical note: an operational landslide early warning

system at regional scale based on space-time-variable rainfall thresholds. *Natural Hazards and Earth System Sciences* 15(4): 853– 861.

Smith A, Dixon N, Meldrum P, Haslam E, Chambers J. 2014. Acoustic emission monitoring of a soil slope: comparisons with continuous deformation measurements. *Geotechnique Letters* 4: 255– 261.

Stahli M, Sattelle M, Huggel C, McCardell BW, Lehmann P, Van Herwijnen A, Berne A, Schleiss M, Ferrari A, Kos A, Or D, Springman SM. 2015. Monitoring and prediction in early warning systems for rapid mass movements. *Natural Hazards and Earth System Sciences* 15(4): 905– 917.

Supper R, Ottowitz D, Jochum B, Kim JH, Romer A, Baron I, Pfeiler S, Lovisolo M, Gruber S, Vecchiotti F. 2014. Geoelectrical monitoring: an innovative method to supplement landslide surveillance and early warning. *Near Surface Geophysics* 12(1): 133– 150.

Take WA, Bolton MD. 2011. Seasonal ratcheting and softening in clay slopes, leading to first-time failure. *Geotechnique* 61: 757– 769
<https://doi.org/10.1680/geot.9.P.125>.

Terzaghi K, 1950. Mechanisms of landslides. *Geological Society of America, Reviews in Engineering Geology*, v 83–123.

Tiranti D, Rabuffetti D. 2010. Estimation of rainfall thresholds triggering shallow landslides for an operational warning system implementation. *Landslides* 7(4): 471– 481.

Toll DG, Lourenço SDN, Mendes J, Gallipoli D, Evans FD, Augarde CE, Cui YJ, Tang AM, Rojas Vidovic JC, Pagano L, Mancuso C, Zingariello C, Tarantino A. 2011. Soil suction monitoring for landslides and slopes. *Quarterly Journal of Engineering Geology and Hydrogeology* 44: 23– 33.

Travelletti J, Sailhac P, Malet JP, Grandjean G, Ponton J. 2012. Hydrological response of weathered clay-shale slopes: water infiltration monitoring with time-lapse electrical resistivity tomography. *Hydrological Processes* 26(14): 2106– 2119.

Tsourlos PI, Szymanski JE, Tsokas GN. 1999. The effect of terrain topography on commonly used resistivity arrays. *Geophysics* 64: 1357– 1363.

Uhlemann S, Wilkinson PB, Chambers JC, Maurer H, Merritt AJ, Gunn DA, Meldrum PI. 2015a. Interpolation of landslide movements to improve the accuracy of 4D geoelectrical monitoring. *Journal of Applied Geophysics* 121: 93– 105 <https://doi.org/10.1016/j.jappgeo.2015.07.003>.

Uhlemann S, Smith A, Chambers J, Dixon N, Dijkstra T, Haslam E, Meldrum P, Merritt A, Gunn D, Mackay J. 2015b. Assessment of ground-based monitoring techniques applied to landslide investigations. *Geomorphology* 253: 438– 451 <https://doi.org/10.1016/j.geomorph.2015.10.027>.

Uhlemann S, Chambers J, Wilkinson P, Maurer H, Merritt A, Meldrum P, Kuras O, Gunn D, Smith A, Dijkstra T. 2017. Four-dimensional imaging of moisture

dynamics during landslide reactivation. *Journal of Geophysical Research - Earth Surface* 122: 398- 418. <https://doi.org/10.1002/2016JF003983>.

Van Asch TWJ, Buma J, Van Beek LPH. 1999. A view on some hydrological triggering systems in landslides. *Geomorphology* 30(1-2): 25- 32.

Varnes DJ. 1978. Slope movement types and processes. In: *Landslides: Analysis and Control, Transportation Research Board*. Special Report 176. National Academy of Sciences. Washington DC, USA, 11-33.

Wilkinson PB, Chambers JE, Meldrum PI, Gunn DA, Ogilvy RD, Kuras O. 2010. Predicting the movements of permanently installed electrodes on an active landslide using time-lapse geoelectrical resistivity data only. *Geophysical Journal International* 183: 543- 556.

Wilkinson PB, Uhlemann S, Chambers JE, Meldrum PI, Loke MH. 2015. Development and testing of displacement inversion to track electrode movements on 3-D electrical resistivity tomography monitoring grids. *Geophysical Journal International* 200: 1566- 1581.